Science of the Total Environment 864 (2023) 161028

Contents lists available at ScienceDirect

Science of the Total Environment

journal homepage: www.elsevier.com/locate/scitotenv

Detention and mapping of iron and toxic environmental elements in human ovarian endometriosis: A suggested combined role

Lorella Pascolo [a,*], Maria Pachetti [a], Anna Camillo [b], Alice Cernogoraz [c], Clara Rizzardi [d], Katarina Vogel Mikus [e,f], Fabrizio Zanconati [d], Murielle Salomé [g], Vanessa Tardillo Suárez [g], Federico Romano [a], Gabriella Zito [a], Alessandra Gianoncelli [h], Giuseppe Ricci [a,d]

[a] Institute for Maternal and Child Health, IRCCS Burlo Garofolo, 34137 Trieste, Italy
[b] Department of Obstetrics and Gynecology, AOUI Verona, Piazzale A. Stefani 1, 37126 Verona, Italy
[c] Department of Gynecology and Obstetrics, F. Del Ponte Hospital, University of Insubria, Varese, Italy
[d] Department of Medical, Surgical, and Health Sciences, University of Trieste, 34149 Trieste, Italy
[e] Jožef Stefan Institute, 1000 Ljubljana, Slovenia
[f] Slovenia Biotechnical Faculty, University of Ljubljana, 1000 Ljubljana, Slovenia
[g] ESRF, The European Synchrotron, 38043 Grenoble Cedex 9, France
[h] Elettra, Sincrotrone Trieste, Strada Statale 14 - km 163,5 in AREA Science Park, Trieste, Italy

HIGHLIGHTS

- Iron nanoaggregates in ovarian endometriosis lesions were analyses by XRF.
- Nano-XRF microscopy revealed deposits of exogenous environmental chemical elements.
- Pollutants like Pb, Br, Ti, Al, Cr, Si and Rb tend to cluster with Fe aggregates.
- Environmental metals may have a role in the diseases.

GRAPHICAL ABSTRACT

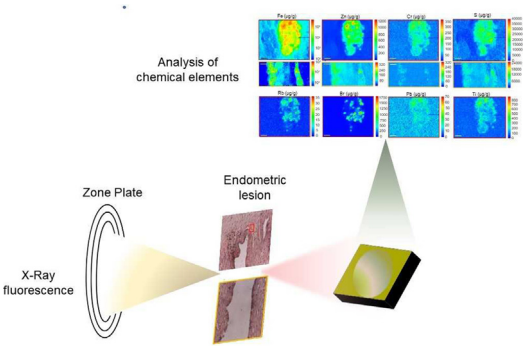

ARTICLE INFO

Editor: Lidia Minguez Alarcon

Keywords:
Endometriosis
X-ray fluorescence
Iron
Environmental metals

ABSTRACT

Background: Endometriosis is a disease affecting 10–15 % of women worldwide, consisting in the ectopic growth of endometrial cells outside the uterine cavity.
Whist the pathogenetic mechanisms of endometriosis remain elusive and contemplating even environmental causes, iron deposits are common in endometrial lesions, indicating an altered iron metabolism at this level. This study was undertaken to reveal a possible relationship between iron dysmetabolism and accumulation of environmental metals.
Methods: By combining histological and histochemical analysis (H&E and Perl's staining) with μ- and nano-synchrotron-based (SR-based) X-ray Fluorescence (XRF) microscopy, we investigated the distribution of iron and other elements in the ovarian endometriomas of 12 endometriosis patients and in 7 healthy endometrium samples.
Results: XRF microscopy expanded the findings obtained by Perl's staining, revealing with an exceptional sensitivity intracellular features of iron accumulation in the epithelial endometrium, stroma and macrophages of the endometriotic lesions. XRF evidenced that iron was specifically accumulated in multiple micro aggregates, reaching concentrations up to 10–20 % p/p. Moreover, by XRF analysis we revealed for the first time the retention of a number of exogenous and potentially toxic metals such as Pb, Br, Ti, Al Cr, Si and Rb partially or totally co-localizing with iron.

* Corresponding author at: Institute for Maternal and Child Health, IRCCS Burlo Garofolo, Via dell'Istria 65/1, 34137 Trieste, Italy.
E-mail address: lorella.pascolo@burlo.trieste.it (L. Pascolo).

http://dx.doi.org/10.1016/j.scitotenv.2022.161028
Received 29 August 2022; Received in revised form 14 December 2022; Accepted 14 December 2022
Available online 20 December 2022

Conclusion: μXRF reveals accumulation and colocalization of iron and environmental metals in human ovarian endometriosis, suggesting a role in the pathogenesis of endometriosis.

1. Introduction

Endometriosis is an estrogen-dependent disease affecting around 10–15 % of women in fertile age in the world, even if the actual prevalence of the disorder is uncertain since the definitive diagnosis requires a surgical visualization (Zondervan et al., 2020). Endometriosis is distinguished by the ectopic growth of endometrial glands and stroma outside of the uterine cavity (Morassutto et al., 2016). Although the disease etiology has not yet been clarified, retrograde menstruation has become the most widely accepted theory for the initial development (Zondervan et al., 2020) Nevertheless, since retrograde menstruation is quite common among females and not all of them suffer from endometriosis, other concurrent conditions should promote the adhesion and the proliferation of endometrial cells in very distant organs such as lungs and brain (Cousins et al., 2018). Additionally, the manifestation of the disease varies among women and may occur as peritoneal lesions, endometrioma, fibrosis and adhesions (Osuchowska-Grochowska et al., 2021). It is well established that ectopic endometrial growth is estrogen-dependent and also an inflammatory process (Patel et al., 2017), with the majority of patients having some degree of endometrial progesterone resistance and hormones influencing the inflammatory response. Additionally, while most manifestations may be originated from an oxidative stress state sustaining the inflammatory condition (Wang et al., 2020), it is generally believed that several factors contribute to the pathogenesis, including environmental factors and a genetic predisposition. In this picture, there is an increasing interest to explore the potential role of exposure to environmental endocrine disruptors in the pathogenesis of this frequent and distressing disease (Smarr et al., 2016).

Increasing studies have suggested a connection between endometriosis and an altered iron metabolism (Bulun, 2009; Defrère et al., 2008; Scutiero et al., 2017; Wölfler et al., 2013), based on the evidence of iron overloads in the many components of the peritoneal cavity of patients with endometriosis. In fact, in endometriosis, frequent bleeding can cause iron accumulation inside endometrial lesions and in peritoneal macrophages.

Few metals such as iron and zinc are physiologically abundant in humans, but toxic effects have been registered only when their delicate concentration balance has been perturbed, inducing their overload in tissues and blood. The non-physiological concentration of these minerals may begin interfering with receptors, initiating the inflammatory condition of the tissues and this could be the case in the endometrium (Darbre, 2006).

Parallel to iron, the presence and accumulation of other chemical elements (even in trace) had been described in the human endometrium since 70', when by means of neutron activation analysis several elements (copper, potassium, rubidium, antimony, zinc, bromine, selenium, sodium, gold, calcium, cobalt and cesium) were measured in both endometrium and deciduas at 12th to 18th weeks of pregnancy. Interestingly, chromium, mercury, silver, and cadmium were found occasionally in the endometrial samples, and still less frequently cerium and scandium, with a small number of samples having traces of arsenic, barium, lanthanum, molybdenum, samarium and strontium, all considered of environmental origin (Hagenfeldt et al., 1977). Some of these metals such as lead, mercury and cadmium can bind to cellular estrogen receptors, mimicking the effect of estrogens (Osuchowska-Grochowska et al., 2021) and for this reason they are classified as metalloestrogens (Defrère et al., 2008; Wölfler et al., 2013). Many of them are not tolerated by humans at any concentration and may accumulate in tissues and organs (Osuchowska-Grochowska et al., 2021), as persistent environmental endocrine disruptors.

To date there are only few studies investigating the effects of these environmental elements on female reproductive tract (Rzymski et al., 2016; Tanrıkut et al., 2014), and more rare those considering their impact in endometriosis (Osuchowska-Grochowska et al., 2021).

To investigate the role of endogenous and exogenous trace elements on endometriosis, most studies explored their content in biological fluids such as blood, urine and peritoneal fluid of patients compared to the healthy population. While some authors did not discover any significant correlation (Pollack et al., 2013), others found a positive correlation between endometriosis and significant amounts of heavy metals, with respect to the healthy population (Choe et al., 2003).

Recently, a systematic review performed by Sirohi et al. summarized the current evidences regarding the environmental exposures to endocrine-disrupting chemicals and their impact on endometriosis. A positive correlation between copper as well as chromium and prevalence of endometriosis, was highlighted, although determined only in one study. In addition, while no clear association was possible with cadmium, lead, and mercury, some intriguing results were reported for the correlation with nickel (Osuchowska-Grochowska et al., 2021; Sirohi et al., 2021).

Differently, very little is known about the content of toxic elements in the ectopic endometrial implants, which could allow to infer eventual causality relation and suggest biological mechanisms in the theory of endometriosis (Osuchowska-Grochowska et al., 2021). Thus, Silva and colleagues reported for the first time the presence of metalloestrogens (nickel, cadmium and lead) in ectopic endometrial tissues of patients with endometriosis (Silva et al., 2012).

The resent work attempted to better investigate the iron overloads as well as the possible appearance of other metals in the endometrial lesions of women affected by endometriosis through the use of X-Ray Fluorescence (XRF) imaging. XRF analysis is a multi-elemental, highly sensitive technique based on the detection of X-rays emitted from sample atoms excited with X-ray photons: under the microscopy modality, it allows characterizing the distribution of elements with subcellular spatial resolution in biological specimens. This technique provides semi-quantitative or quantitative information, since the intensity of fluorescence is related to the concentration of the element within the sample. Although theoretically all chemical elements are detectable by XRF, the elemental sensitivity depends from the incident energy and on their concentration. Over the past decade, the investigation of biological samples with XRF (Kaulich et al., 2009; Ortega et al., 2007; Pascolo et al., 2013; Paunesku et al., 2006) has been favored by the development of high-flux and highly focused X-ray beams at different synchrotron facilities. As already proven by our group and by previous studies from other authors, formalin-fixed paraffin-embedded (FFPE) tissues are ideal samples to be analyzed with this technique since the treatment preserves their morphology and XRF detection of most endogenous elements can be conducted without altering the elemental distribution (Paunesku et al., 2012; Ralle and Lutsenko, 2009).

In the present paper, we used synchrotron XRF to analyze twelve FFPE samples of human ovarian endometriomas and seven FFPE samples of healthy endometrial controls. We demonstrated a high accumulation of trivalent iron and significant deposits of exogenous chemical elements in the tissues collected from patients diagnosed with endometriosis, while low levels of iron and no accumulation of environmental elements was found in the healthy endometrium samples (controls).

2. Materials and methods

2.1. Patients and tissue samples

Endometriosis and control patients undergoing conservative laparoscopy were enrolled at the Department of Obstetrics and Gynecology of the Institute and the study was approved by the regional (FVG) Ethics

Committee (CEUR-2021-Os-168). The exclusion and inclusion criteria were evaluated by the Ethical Committee. Women excluded from the study were below 18, or suspected for any ovarian or uterine malign neoplasia, or with chronic diseases, or with infectious diseases (viral and bacterial). Additionally, women with diseases related to iron metabolism or that had taken medicines containing iron during the 3 months prior the study or with recent transfusions were excluded as well. As reported in Table 1, patients affected by endometriosis (12 cases) were selected with the following criteria: they were aged between 18 and 40 years, with regular menstrual cycle, and carrying uni- or bi-lateral symptomatic ovarian endometriomas ≥ 3 cm in diameter. The endometriosis stage was assessed according to the criteria of the American Fertility Society (Wiegerinck et al., 1993). Tissue samples from endometriotic lesions were obtained after written consent from patients with surgical resection of ovarian endometriotic cysts, while endometrium used as control was obtained from seven patients of similar ages (ages up to 50 years were tolerable for subjects with regular menstrual cycle) undergoing surgery for benign gynecologic pathologies. Formalin-fixed, paraffin-embedded tissue samples were obtained from surgical resection specimens.

2.2. Histological analyses and Perl's staining

For the histological analysis, samples containing both endometrial type glands and endometrial type stroma were chosen. The diagnosis of endometriosis and the selection of the areas to be analyzed were performed by light microscopy (Leica Microsystems, Germany) on 3 μm-thick sections of paraffin-embedded samples stained with hematoxylin and eosin (H&E), according to the standard protocol. Perl's staining was performed as previously reported in (Pascolo et al., 2015).

For X-ray imaging and XRF analyses, 5 μm-thick sections were obtained from the selected tissue areas, mounted on ultralene foils (4 μm-thick) and air-dried, as previously described (Pascolo et al., 2014). XRF analyses were performed randomly choosing among Perl's positive regions.

2.3. X-ray fluorescence (XRF) spectroscopy and analysis

The synchrotron XRF analyses have been performed at three different synchrotron beamlines. In all cases, the X-ray beam was focused on the sample through appropriate optics and the sample was raster scanned to collect the emitted X-ray Fluorescence (XRF) by means of energy dispersive silicon drift detectors.

2.3.1. Micro-XRF elemental analysis at ID21 (7.3 keV)

Some samples were initially analyzed at ID21 beamline of the European Synchrotron Radiation Facility (ESRF, Grenoble, France). Briefly, the 7.3 keV monochromatic X-ray beam was focused onto the sample using Kirkpatrick-Baez mirrors (KB) with a spot size of 0.85 μm × 0.58 μm (H × V) and with a photon flux of 5.2×10^{10} photon/s/Si(111) bandwidth. The acquisition time was typically 300 ms/pixel with a step size of 500 nm.

2.3.2. Nano-XRF elemental analysis at ID16B (17.2 keV)

Other samples were analyzed at the ID16B-NA beamline (Bissardon et al., 2019) of the European Synchrotron Radiation Facility (ESRF, Grenoble, France) where the pink ($\Delta E/E = 0.01$) 17.2 keV X-ray beam was focused by Kirkpatrick-Baez (KB) mirrors to a spot size of 60 nm × 60 nm on the sample plane (photon flux $4 * 10^{10}$ photons/s). The XRF emitted by the sample were collected by two SGX sensortech SDD arrays, each with an active silicon area of 80 mm^2, using an acquisition time of 100–200 ms per pixel in the raster scan and a step size of 100 nm. A standard reference material from NIST (bovine liver SRM 1577B) was measured for calibration of the XRF spectra to get semi-quantitative results on transition metals. Spectra were fitted based on the configuration derived from the measured standard using PyMCA software (Sole et al., 2007) for quantification of the elemental content. The obtained concentrations are expressed in μg/g assuming a 1.5 μm thick protein matrix with density 1.2.

Quantification of the 2D maps was performed according to Kump et al. (Kump and Vogel-Mikuš, 2018). Calibration of the system was carried out with pure metal foils obtained from Micromatter (Canada). The geometric constant was calculated based on fundamental parameters and pure metal foil intensities. The procedure was validated using certified reference materials (Koren et al., 2013; Kump and Vogel-Mikuš, 2018).

2.3.3. X-ray microscopy and LEXRF at TwinMic

Some samples, previously investigated at other XRF beamlines, were analyzed under a low energy microscopy set-up at the TwinMic beamline (Elettra – Sincrotrone, Trieste, Italy) (Gianoncelli et al., 2016). TwinMic microscope operated in scanning transmission mode (STXM) with the beam focused on the sample through a zone plate diffractive optics providing sub-micron spatial resolution. At TwinMic the absorption and phase contrast images outline the morphological features of the sample at sub-micrometer length scales (Gianoncelli et al., 2006), whereas the

Table 1
The list of the biological samples analyzed along with clinical details regarding patient age, Body Mass Index (BMI) diagnosis, grade of the lesions and the analyses performed.

Case	Age	BMI	Description	Stage	Analysis
A1	35	21	Ovarian endometriotic cyst	III	HE, Perl's, XRF
A2	28	21	Ovarian endometriotic cyst	III	HE, Perl's
A3	29	16	Ovarian endometriotic cyst	IV	HE, Perl's, XRF
A4	24	20	Ovarian endometriotic cyst	IV	HE, Perl's
A5	32	21	Ovarian endometriotic cyst	III	HE, Perl's
A6	40	19	Control		HE, Perl's, XRF
A7	27	20	Ovarian endometriotic cyst	III	HE, Perl's, XRF
A8	34	29	Ovarian endometriotic cyst	III	HE, Perl's
A10	31	33	Ovarian endometriotic cyst	III	HE, Perl's
A11	50	28	Control		HE, Perl's
A12	42	24	Ovarian endometriotic cyst	IV	HE, Perl's
A13	47	24	Control		HE, Perl's
A14	45	29	Control		HE, Perl's
A15	40	26	Control		HE, Perl's
A16	21	23	Ovarian endometriotic cyst	IV	HE, Perl's
A18	40	18	Ovarian endometriotic cyst	III	HE, Perl's, XRF
A19	27	22	Ovarian endometriotic cyst	III	HE, Perl's
A20	46	37	Control		HE, Perl's
A21	42	24	Control		HE, Perl's

Type	Age (±SD)	BMI (±SD)
Control group	44 ± 4	27 ± 6
Case group	31 ± 6	22 ± 2

Table 2
Perl's positivity and localization of trivalent iron aggregates in the samples analyzed.

Sample	Nr.	Epithelium	Stroma	Siderophages	Epithelium + stroma + siderophages
Ovarian cyst	12	3 (25 %)	2 (17 %)	–	6 (50 %)
Control	7	–	–	1 (14 %)	–

simultaneous detection of the low energy XRF (Gianoncelli et al., 2013, 2009) correlates the elemental distribution to the morphology. For the present experiments, we selected a photon energy of 2 KeV to excite and get optimal emission conditions for the elements of major interest, namely Si and Mg and O, with a spot of 400 nm, delivered by a 600 μm diameter Au zone plate with 50 nm outermost zone, and a dwell time of 14 s and a photon flux of around 3×10^7 photon/s. The sample was mounted on an x-y stage (with the incoming beam perpendicular to the sample surface) facing eight Silicon Drift Detectors placed at 2.8 cm from the sample (Gianoncelli et al., 2013). All XRF spectra acquired were processed by using PyMCA software package (Sole et al., 2007), producing XRF maps highlighting the distribution of the detected chemical elements.

3. Results

3.1. Histological analysis

Hematoxylin and eosin staining of histological samples was used to identify the different components of endometrial lesions in all the 12 patients affected by endometriosis (see example in Fig. S1 in supporting material) and to evaluate the morphological features of endometrial components belonging to the 7 controls (see Table 2) (images not shown).

Perl's staining, which detects the ferric ions (valence 3+), was performed with several repetitions; Fe^{3+} was clearly revealed at high concentration in many endometriotic cells (epithelial and stromal) and rare macrophages. Representative results of the staining in three different samples are reported in Fig. 1, showing that iron accumulation is mostly concentrated in the glandular epithelium (panels a, b), inside the stroma (panels c, d), and inside macrophages (panels e,f), respectively. Table 2 reports the Perl's positivity of all the samples divided on the basis of Fe^{3+} localization. Interestingly, of the 12 ovarian cysts examined, 3 showed ferric deposits in the epithelial cells, 2 in the stroma, 1 showed positivity only in the macrophages and 6 showed that iron was present in more cell types. Only one cyst was negative for Perl's staining. The controls were almost negative for the staining, with the exception of one case that showed rare positive siderophages (images not shown). The results are in line with what has been already reported in previous studies (Scutiero et al., 2017).

3.2. XRF microscopy and analysis at ID21 (7.3 keV)

Synchrotron X-ray fluorescence microscopy was used to investigate the elemental distribution and composition together with the morphology of human ovary tissues. The analysis of the ovarian tissue slices conducted at ID21 (7.3 keV), with a sub-micron spatial resolution, reported a well-defined pattern of multiple cell types together with a clear distribution of several chemical elements (Ca, P, Si, Ti, Cr) and Fe.

Fig. 2 shows an example of XRF analysis performed on the endometrial tissue of patient A18. As already evidenced by Perl's staining (Fig. 2b), XRF analysis highlighted the presence of iron in proximity and along the endometrial lesion and in macrophages. XRF analysis showed the iron distribution with an increased sensitivity compared to Perl's staining, and this element seems to reach extremely high levels in the epithelial layer but also start to diffuse in the stroma underneath. Interestingly, other metals such as Si (panel f), Mn (panel i) and Ti (panel l) accumulated in the region where iron is found. K and S were not informative on the characteristics of the lesion, as they simply delineated the tissue morphology; P was used to recognize different cells present in the tissue.

The XRF analysis on endometriotic stromal tissue of patient A18 is presented in Fig. 3. The distribution of Fe, Mn, Al, Cl, Cr, Si and Ti highlighted the presence of two macrophages (indicated through black and red arrows). Only Fe accumulated in both cells at a significant amount, while other elements were present in trace amounts. Similarly to what occurred for the epithelial region reported in Fig. 2, Fe, Si, Ti and Mn co-localized in the macrophages.

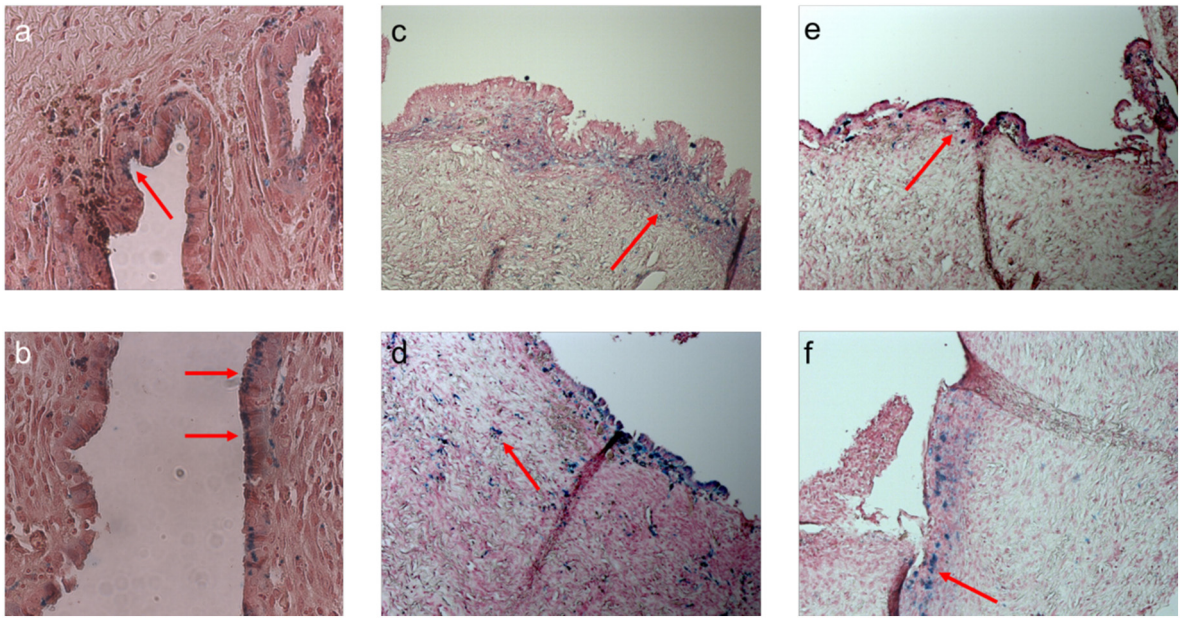

Fig. 1. Visible light images of Perl's stained samples of endometrial lesions reporting the different distribution of trivalent iron; in particular, Fe^{3+} is concentrated mostly in (a, b) the glandular epithelial component (patient A1), (c) inside the stroma (patient A3), (d) both in the epithelium and inside the stroma (patient A10) and (e, f) mainly inside macrophages as indicated by red arrows (patients A18 and A19, respectively).

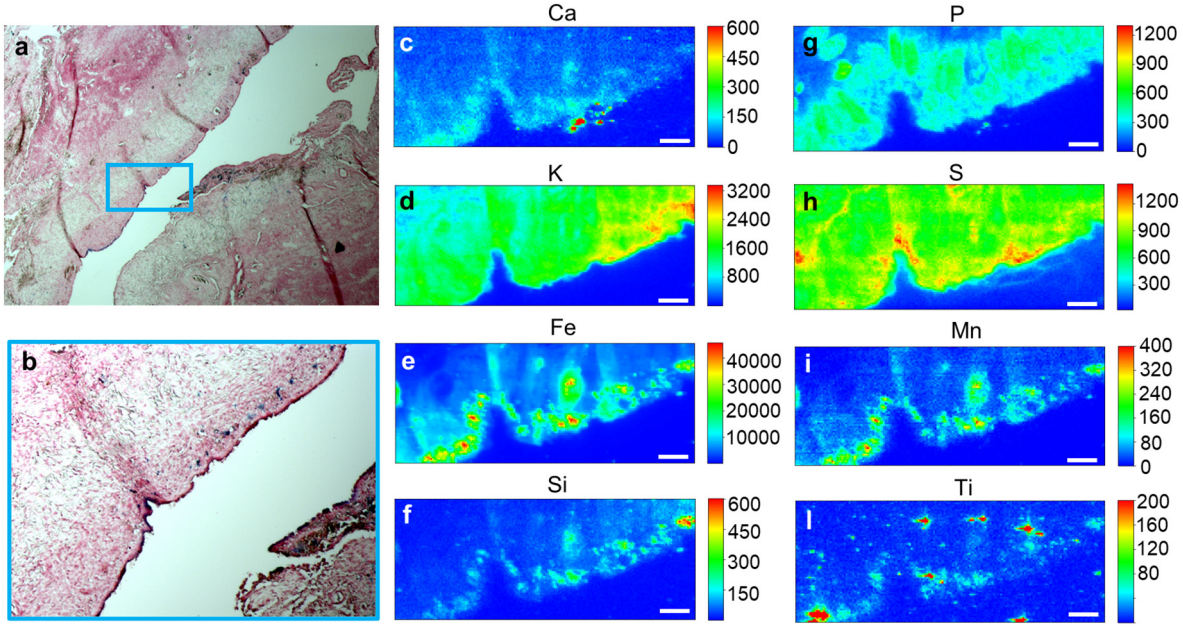

Fig. 2. Photos of Perl's stained tissue with (a) 2.5× and (b) with 10× magnification (of the selected region enclosed in the cyan box). X-ray fluorescence (XRF) intensity maps of (c) Ca, (d) K, (e) Fe, (f) Si, (g) P, (h) S, (i) Mn and (l) Ti were collected at 7.3 keV with a step size of 500 nm and 300 ms/pixel acquisition time. Scale bar is 20 μm.

3.3. XRF microscopy and analysis at ID16 (17.2 keV)

In order to reach nanoscale spatial resolution and also increase the number of detectable chemical elements, the investigation of the ovarian endometriotic tissues was furtherly performed at ID16B-NA beamline (ESRF, Grenoble, France) only on a selected number of patients. For each analyzed sample, fast and low resolution XRF images were initially obtained from adjacent areas of 80 × 80 μm^2, to be reconstructed and compared with the pertinent Perl's and/or hematoxylin and eosin images.

Firstly, the normal endometrium controls were evaluated, and the hematoxylin and eosin (panels a and b), Perl's (panels c and d) images and the XRF maps of Zn and Fe (panels e, f and g, h, respectively) are reported in Fig. 4.

Both Perl's staining (Fig. 4c and d) and XRF maps of the control sample (4 g and h) did not evidence the presence of high amounts of Fe, which is thus characteristic of endometriosis. Additionally, the presence of other metals in the controls was negligible (Fig. S2 in supporting information).

The same analysis was carried out for an endometriotic lesion of patient A1: the hematoxylin & eosin image and the XRF maps of Fe and Zn are reported in Fig. 5 panels a, b and c, respectively. The whole XRF map of the lesion is reported in Fig. 5 panel a, obtained by assembling single XRF adjacent maps of 80 × 80 μm^2 selected in the area of interest. As clearly shown in Fig. 5 panel b, the distribution of Fe mostly regarded endometrium, spanning from the inner part of the lesion to the endometrial stroma. Differently from Perl's staining that can be affected by artifacts related to the operator's handling, and is able to detect only high levels of iron, XRF technique

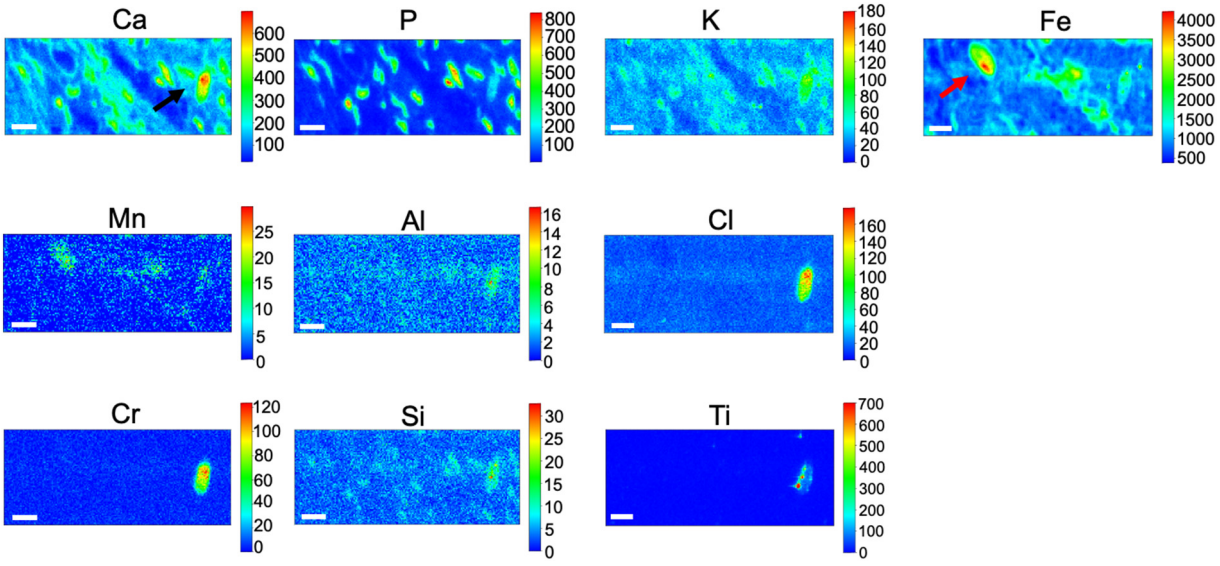

Fig. 3. X-ray fluorescence (XRF) Intensity maps of Ca, P, K, Fe, Mn, Al, Cl, Cr, Si and Ti of a selected region of endometriotic stromal tissue reporting the presence of two macrophages, highlighted with black and red arrows. All the XRF maps were collected at 7.3 keV with a step size of 500 nm and 300 ms/pixel acquisition time. Scale bar is 20 μm.

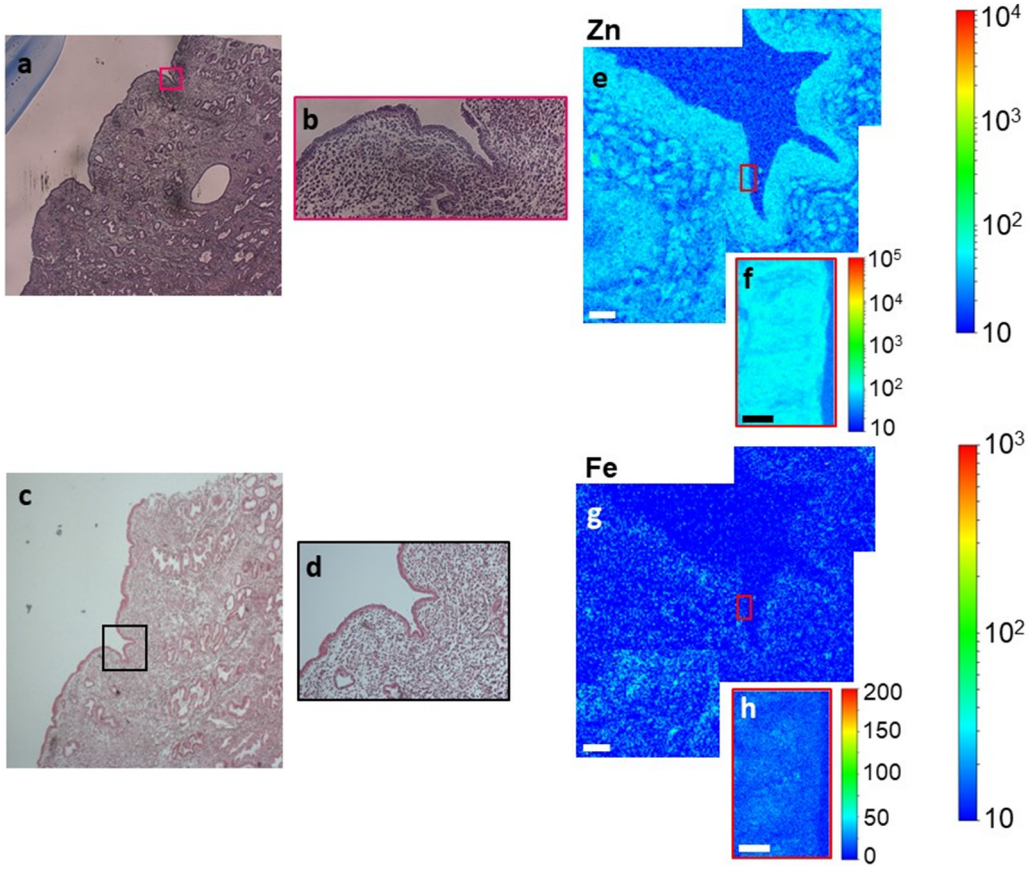

Fig. 4. Visible light images of hematoxylin and eosin stained tissue of control patient A6 with (a) 2.5 x and (b) with 10× magnification (selected region). Visible light images of Perl's stained tissue with (c) 2.5× and (d) with 10× magnification (selected region). Panels e and g depict XRF intensity maps of Zn and Fe respectively, while f and h show the high resolution Zn and Fe map respectively of the inset indicated with the red box. All the XRF maps were collected at 17.2 keV with a step size of 100 nm and 100-200 ms/pixel acquisition time. Scale bar is 20 μm in panels e and g, while 5 μm in panel f and h.

demonstrated an exceptional sensitivity and specificity in revealing the distribution of iron in a semi-quantitative manner. The distribution of zinc indicated that this element is quite uniformly distributed along the lesion and surrounding tissue, being not so different to the levels found in the controls (i.e. patient A6 reported in Fig. 4). Interestingly, increased levels of Zn are helpful in the identification of macrophages dispersed in the tissue.

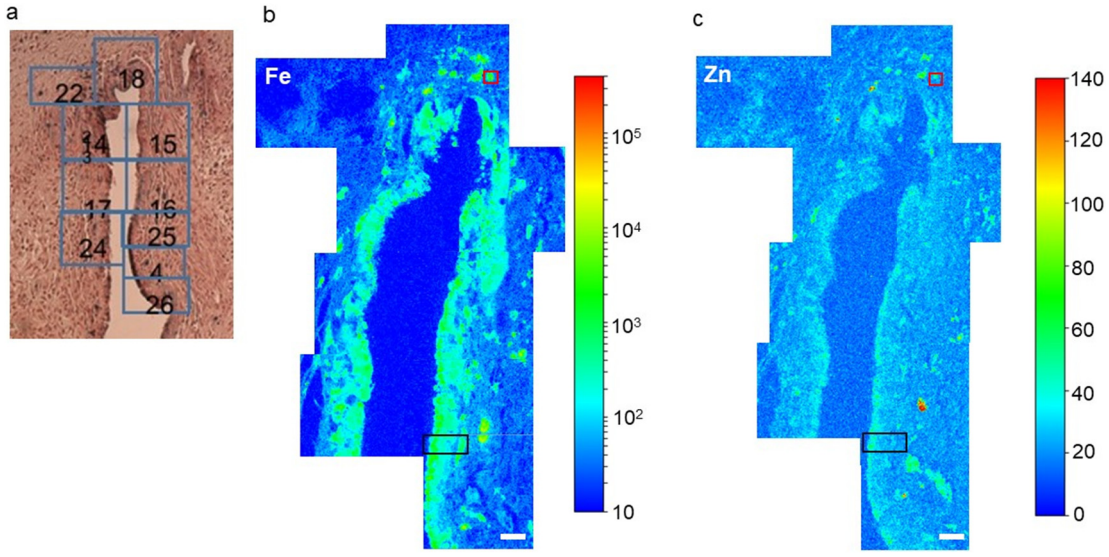

Fig. 5. Visible light image of (a) Perl's stained tissue of A1 sample with x magnification. X-ray fluorescence (XRF) maps of (b) Fe and (c) Zn. All the XRF maps were collected at 17.2 keV with a step size of 100 nm and 100-200 ms/pixel acquisition time. Scale bar is 20 μm (white line).

Fig. 6 reports the semi-quantitative XRF analysis (levels expressed in μg/g) performed on two peculiar regions of the lesion, highlighted in Fig. 5 (panels b and c) by a red and a black box.

Fig. 6 panels (a-i) shows the semi-quantitative XRF maps of a macrophage identified from the low-resolution Fe and Zn maps reported in Fig. 5 (panels b and c), based on the clear morphology and elemental content. Apart from the highly abundant Fe, the analysis revealed the accumulation of Br, Pb, Rb and Ti in microscale aggregates, partially co-localized with the distribution of Fe. In particular, Br seemed to have a peculiar spot-like distribution compatible with intracellular vesicles, partially co-localizing with Rb. To note, Rb could not be precisely quantified since the signal was close to the limit of detection.

Similarly, Fig. 6 panels (j-o) report the semi-quantitative XRF maps of a portion of ectopic endometrium. Interestingly, iron distribution has a concentration lower than 0.1 % in unaffected tissue, but reaches values up to 20 % (200,000 μg/g) in many spots inside the epithelial cells as well as in some stromal cells or macrophages. A curious granular appearance of the iron aggregates was depicted only in epithelial cells, with the signal being

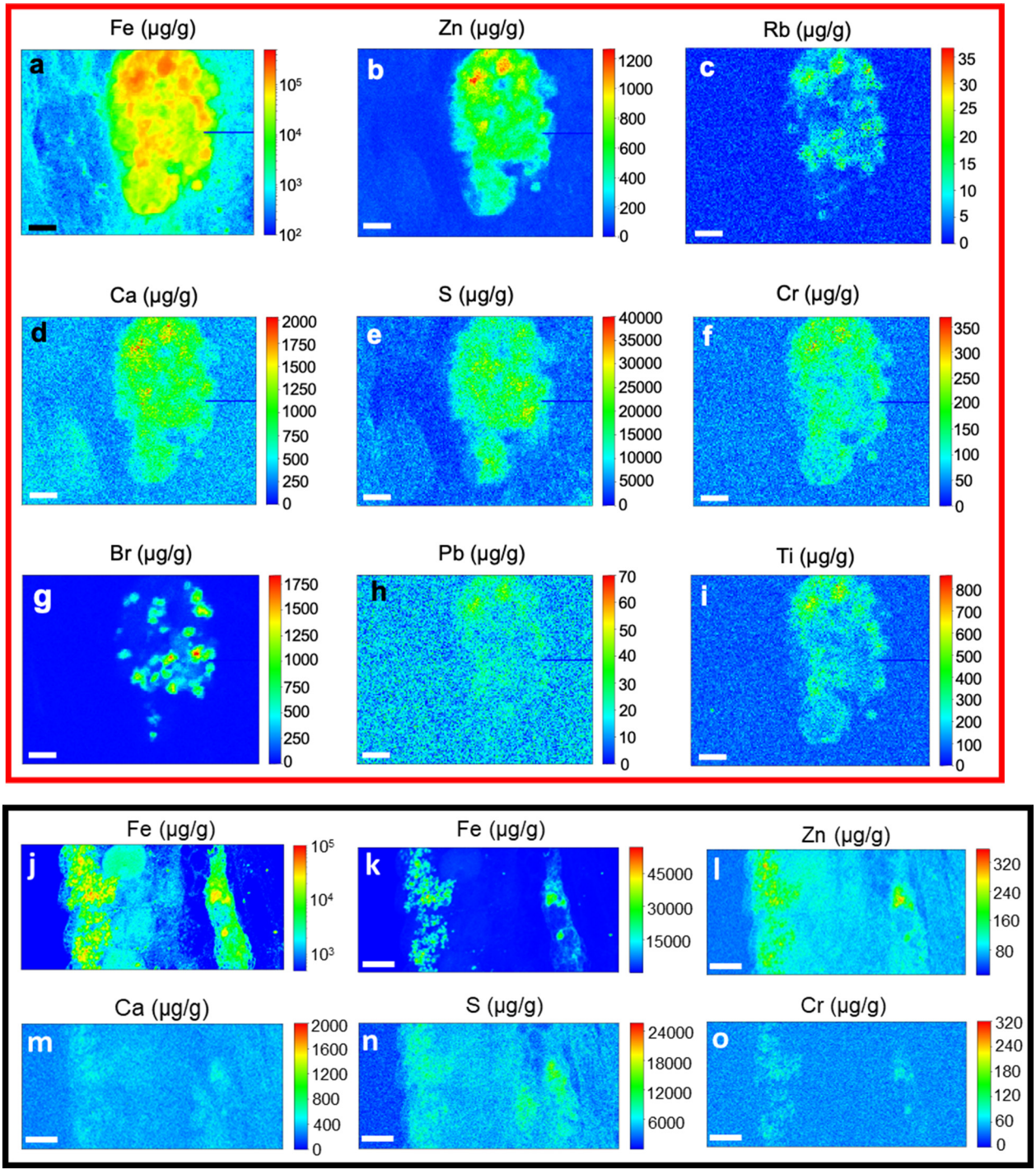

Fig. 6. Quantitative analysis (except for Rb) of two selected regions of patient A1, indicated with a red and a black box in Fig. 5, panels b and c). For the red box region (a) Fe, (b) Zn, (c) Rb, (d) Ca, (e) S, (f) Cr, (g) Br, (h) Pb, (i) Ti could be quantified (scale bar 2 μm). For the black box area Fe in (j) logarithmic scale and (k) linear scale, (l) Zn, (m) Ca, (n) S, (o) Cr could be retrieved (scale bar is 5 μm,). Both areas were scanned at 17.2 keV with 100 nm step size.

more homogeneous in other districts. Of particular interest, the levels of Br, Pb and Ti in this region were too low to be detected, and these elements likely accumulated in macrophages. An intriguing co-localization of Cr in nano- to micro-scale aggregates was be pointed out by XRF analysis, especially where Fe levels were the highest.

Differently, Fig. 7 reports the example of an endometrial lesion of patient A3 where Fe seemed mainly concentrated in the stroma (see (c) and (d)). This conclusion was partially confirmed by the distribution of Fe in the XRF map (see (f)), where a more diffused pattern of the metal spanning inner ward from the stroma was highlighted. The distribution of Zn (see panel e) was quite uniform, not distinguishing the lesion borders, while increased levels could identify the presence of red blood cells that were abundant in this sample.

A peculiar distribution of Fe both in the epithelial region and in the stroma can be found in patient A7 and it is reported in Fig. 8 (panel f). As previously reported, the distribution of Zn followed an intriguing pattern, being more concentrated in some structures of the stromal portion (see panel e). Additionally, panels (g-k), which are a sub-region of panels e and f, highlight a co-localization of both Br and Rb similarly to what have been shown for the macrophages of patient A1 (see Fig. 6). Differently, in this case, the co-localisation of Br and Rb did not follow the distribution of Fe (see panels g-k) even if the highest content of these metals resided in an iron-rich region.

High-resolution XRF images of a selected region in the sample of patient A7 are reported in Fig. 9 (panels a-e), showing the semi-quantitative analysis of endogenous elements and other metals accumulated in the tissue. As reported before, the iron signal was extremely high in the epithelial and stromal cells, presenting some spots of well-defined shapes compatible with the presence of erythrocytes. The presence of Br was intriguing and its distribution did not follow the iron one, confirming what was already observed for other patients. No significant amount of Rb was detected in this region.

3.4. XRF microscopy and analysis at TwinMic (2 KeV)

Fig. 10 shows the results of Soft X-ray Microscopy combined with Low Energy XRF (LEXRF) mapping performed at the TwinMic beamline (Elettra Sincrotrone Trieste, Trieste, Italy), where a photon energy of 2 keV was chosen for optimal excitation of Si and Al. The absorption and phase contrast images disclosed the morphology of the ectopic endometrium, distinguishing the epithelial layer from the rest and revealing highly absorbing segments with increased iron occurrence (data not shown). Interestingly these dense structures revealed an abundant presence of Si and Na, confirming the analyses at ID21 beamline. In addition, Al was revealed at significant levels, following a spot-like distribution in all analyzed regions. Differently, Mg did not reveal any particular distribution.

4. Discussion

Iron overload in ectopic lesions linked to endometriosis has been already pointed out, and considered by many authors as associated with an increased risk of infertility (Mori et al., 2015) and of developing tumors (particularly ovarian cancer (Rockfield et al., 2017), being iron a major pathogenic factor for carcinogenesis (Nakamura et al., 2019; Ying et al., 2021). Although the causes of endometriosis are still not explained, the role of iron and the meaning and consequences of its deposits in ectopic and also endometrial lesions has to be further investigated, also as potential target of therapeutic approaches. Iron overload does not seem to affect lesion establishment but could contribute to the further growth by promoting cellular proliferation within lesions. For this reason, there is a rational for iron chelator treatment to prevent iron overload in the pelvic cavity and decrease cellular proliferation in the lesions. (Ng et al., 2020).

Our observational and pilot study has been conducted on 12 patients clinically diagnosed with endometriosis, and on 7 controls. As reported in Tables 1 and 2, 11 over 12 tissues with endometriosis were positive to

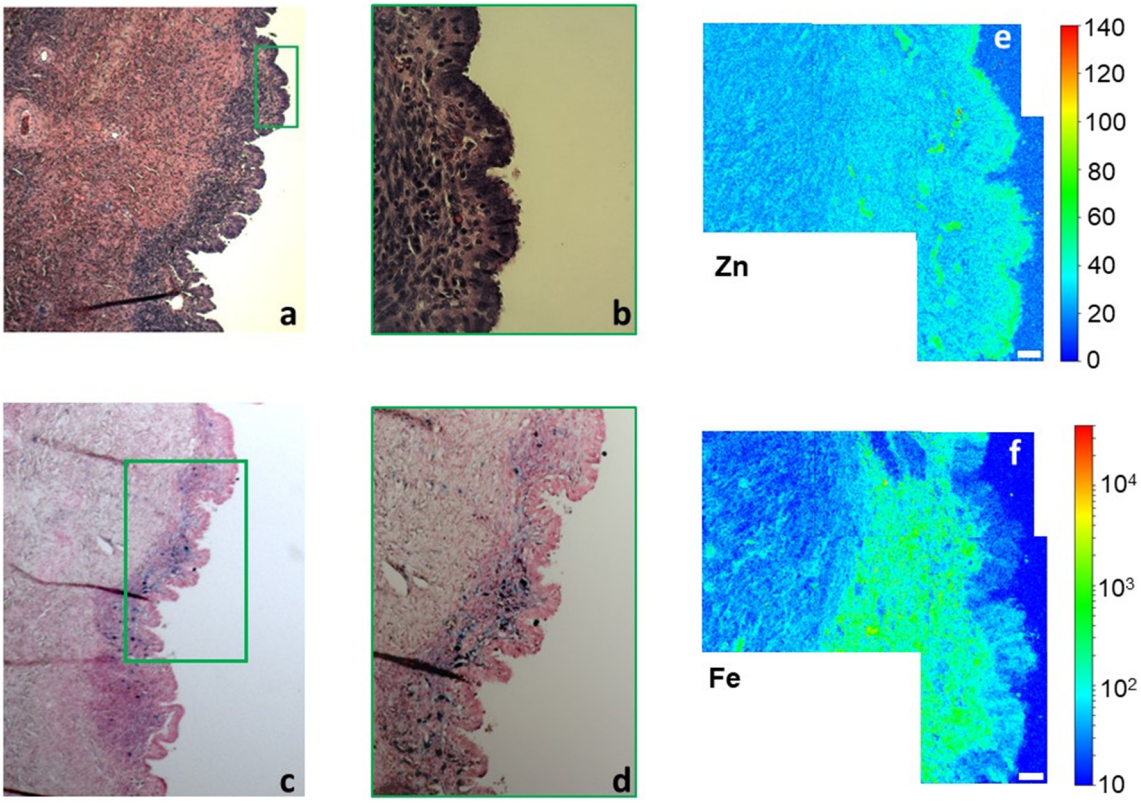

Fig. 7. Visible light images of hematoxylin and eosin stained tissue of A3 sample with (a) 2.5× and (b) with 10× magnification (selected region). Visible light images of Perl's stained tissue with (c) 2.5× and (d) with 10× magnification (selected region). X-ray fluorescence (XRF) maps of (e) Zn with a scale bar of 20 μm (white line) and of (f) Fe collected at 17.2 keV with a step size of 100 nm and 100-200 ms/pixel acquisition time. Scale bar of 20 μm.

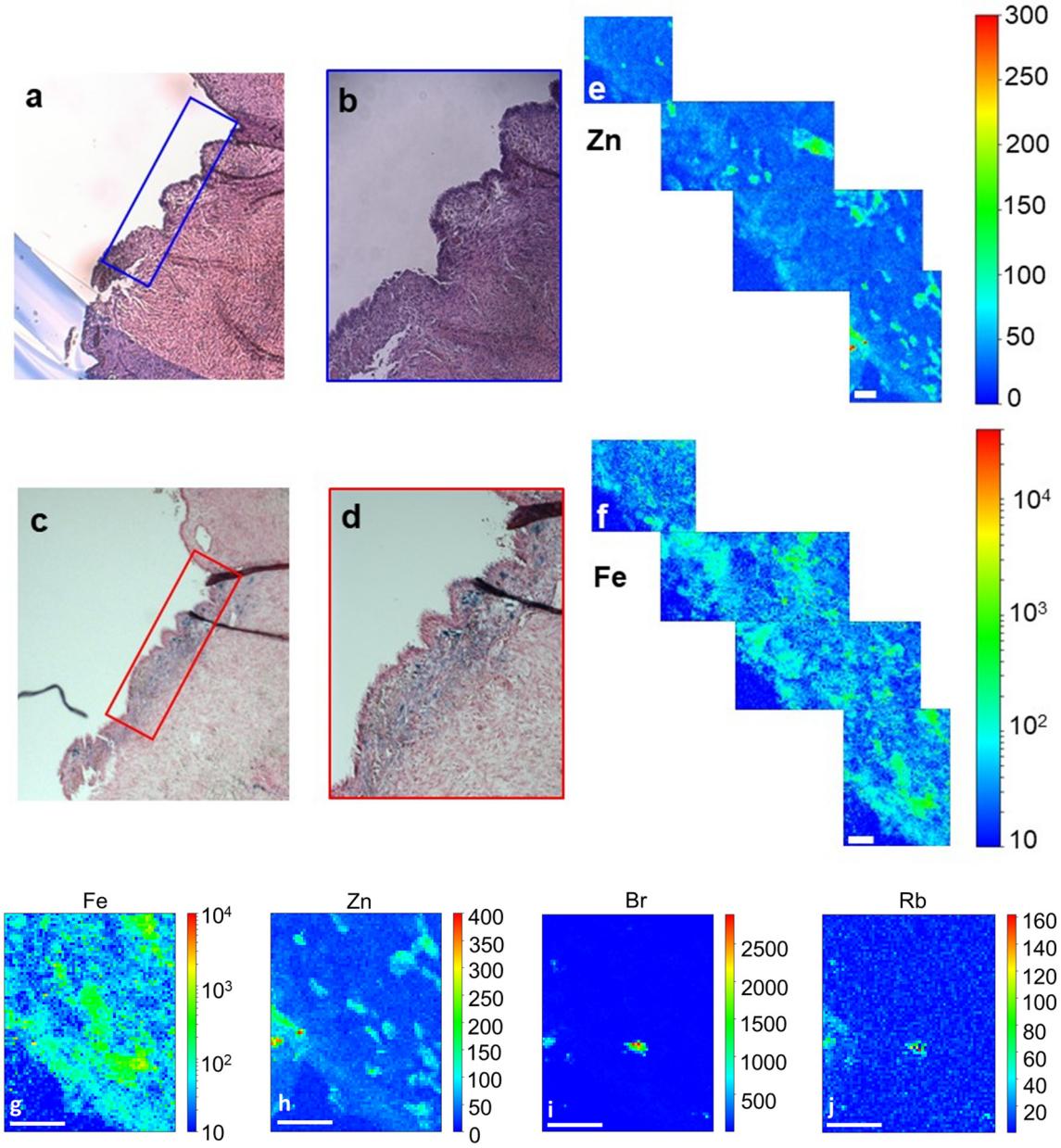

Fig. 8. Visible light images of hematoxylin and eosin stained tissue of A7 sample with (a) 2.5× and (b) with 10× magnification (selected region in (a)). Visible light images of Perl's stained tissue with (c) 2.5× and (d) with 10× magnification (selected region in (c)). XRF intensity maps of Zn (e) and Fe (f). XRF images of a selected area of panels e-f showing the distribution of (g) Fe, (h) Zn, (i) Br and (j) Rb. All the XRF maps were collected at 17.2 keV with a step size of 100 nm and 100-200 ms/pixel acquisition time. Scale bar of 20 μm.

Perl's staining, confirming the presence of significant Fe^{3+} deposits in the histological samples. The specificity of Perl's in staining Fe^{3+} is conventionally used to reveal pathological iron deposits of ferritin and hemosiderin, both in affected parenchymal tissues and siderophages, while being poorly effective in revealing the metal at moderately increased levels (Pascolo et al., 2015). As expected, the endometrial controls do not show Perl's positivity and Fe^{3+} deposits. Our results are comparable to what reported by (Ovarian endometriosis-associated stromal cells reveal persistently high affinity for iron (Mori et al., 2015). Nonetheless, a more specific picture of iron distribution in the samples has been reached through the analysis of the XRF images collected at ID21 and ID16 beamlines at ESRF. Although the XRF technique is not able to distinguish the chemical state of the iron in the tissue, it offers a label- and bias-free method with an outstanding sensitivity that cannot be reached by common histochemical analysis. Summarily, the iron distribution reported in the XRF images is quite comparable to that obtained by Perl's staining. However, through the XRF elemental mapping analysis, we observed that excess iron is not only distributed in the epithelial region close to endometrial cysts, but it also spreads towards the stroma, being present at high concentration within macrophages, and also reaching the fibrotic tissue underneath with substantial levels.

Quantitative XRF analysis revealed that iron deposits reach concentrations of 10–20 % p/p in multiple microspots. Interestingly, similar levels of iron have been reported in other pathological conditions such as hepatic siderosis and asbestosis (Delfino et al., 2011; Ito et al., 2021; Milic et al., 2016). This observation fosters the concept that iron overload represents a very stressful condition, exposing tissues to a strong oxidative stress (i.e. production of reactive oxidative species) and inflammation (Ying et al., 2021). It is well known that Reactive Oxidative Species (ROS) are responsible for cellular lipid peroxidation, a chemical condition that alters cellular membranes' functionality and also interferes with molecular pathways such as that involving NF-kB. More, ROS are able to alter some regulatory

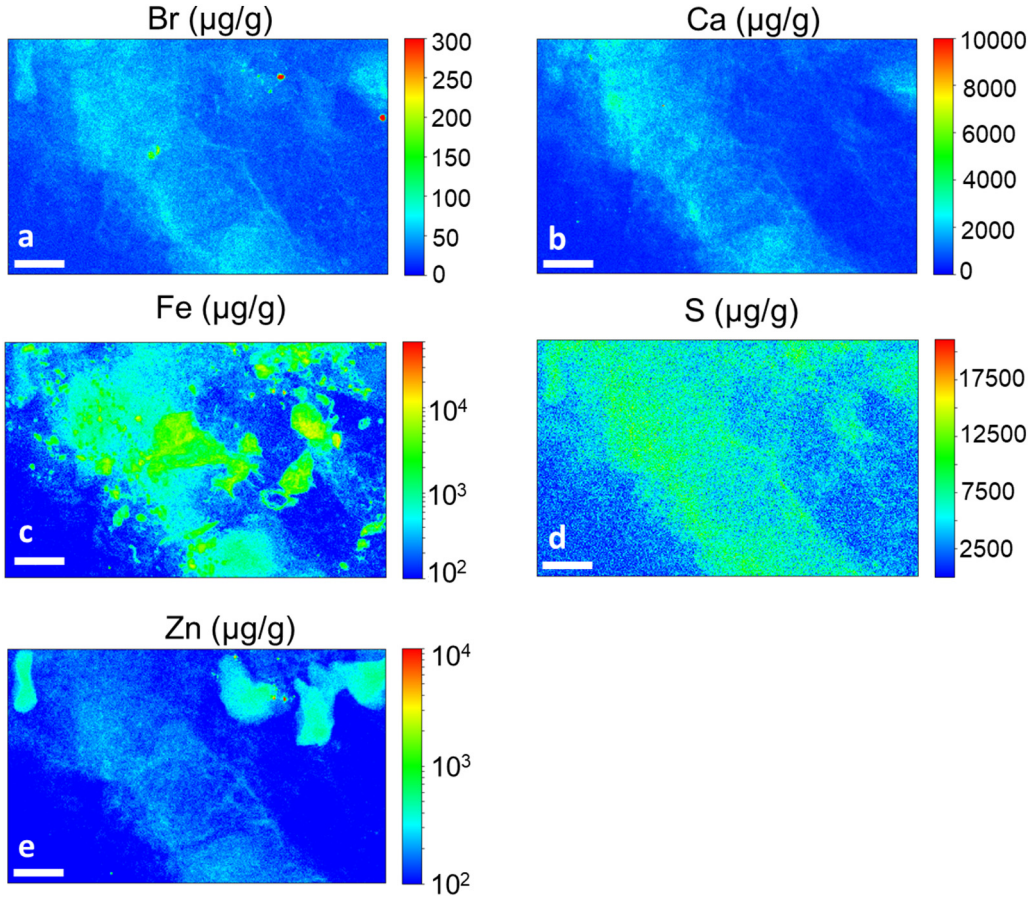

Fig. 9. Quantitative high-resolution XRF maps of (a) Br, (b) Ca, (c) Fe, (d) S, (e) Zn. Scale bar is 5 μm. All the XRF maps were collected at 17.2 keV with a step size of 100 nm and 100-200 ms/pixel acquisition time.

genes such as those involved in the inflammation control and in the cellular proliferation (González-Ramos et al., 2012).

Parallel to iron, the combination of three different XRF set-ups and energies in our study allowed to get optimal excitation of a wide range of chemical elements such as Pb, Br, Ti, Al, Cr, Si and Rb in the tissues of patients affected by endometriosis. The presence of these exogenous elements, some of them well known as metalloestrogens, totally or partially accumulated in those regions where iron concentration is the highest, suggesting that they may be linked to iron dysregulation, as suggested in other contests for toxic metals (Ghio et al., 2012; Maximova et al., 2016; Wang and Xia, 2015), also by our group (Delfino et al., 2019; Pascolo et al., 2015). In addition, they may play a role in worsening the inflammation, and endorses the theory of endometriosis with environmental pollution (review EEC) acting on the onset and/or in the progression of the disease (Rzymski et al., 2015). From the quantitative analysis of XRF images, we pointed out that the levels of some metals are undoubtedly significant (like Cr and Pb with μg/g) to possibly have a role in the production of ROS or on cellular receptors. Interestingly, the metals are not only concentrated within macrophages (see Figs. 3 and 6), mainly involved in the absorption and discharge of toxic elements from the organism, but also within the epithelial and stromal cells of pathological endometrium (see Figs. 3 and 6) where these elements may function as metalloestrogens.

It is difficult to compare our results to previous studies regarding the appearance of trace exogenous metals in endometrial tissues or other body districts: even more complicated to estimate if our quantities are significant to have really a biological role. In fact, our data are under imaging modality that only a few advanced techniques can give, implying unprecedented information on the specific cellular localization. Considering however that the quantitative resolution of XRF is low, with a detection limit of few ppm, we probably failed to reveal the background concentration that can be found also in non-pathological (control) tissues. Recently, Rzymski and colleagues (Rzymski et al., 2016) published that the average concentration of heavy metals found in smokers spanned from 3.5 to 20 μg/kg in dry healthy endometrial tissues: interestingly our data show that much higher concentration (tens of μg/g) are achieved in single cells or internal aggregates (i.e. Cr is about 40 μg/g, and Pb is 5–10 μg/g in the macrophage of Fig. 6).

Although this paper demonstrates the presence of iron and other metals in tissues collected from patients diagnosed with endometriosis has been demonstrated by the present paper, the mechanism through which these metals were found accumulated in ectopic endometrial cells is unknown as well as the pathway through which they can come across the cellular membranes. Finally, among the mechanistic hypothesis, we cannot exclude that the retention of toxic metals in the tissues is partially consequence of highly vascularized lesions, although not all the lesions present this characteristic (Brosens et al., 2004).

The present questions represent a starting point for further studies, willing to investigate the role of these environmental elements in the progression or in the onset of hormone-mediated diseases, such as endometriosis.

5. Conclusions

The combination of XRF imaging at different excitation energies together with histochemical analysis, revealed novel features of the iron overload in the ovarian ectopic lesions of patients affected by endometriosis. Notably, iron concentration can reach extremely high concentrations even up 10–20 % p/p in several micro-spots alongside the lesions. Additionally, thanks to the powerfulness of XRF microscopy analysis, we revealed the occurrence of exogenous and toxic chemical elements in different cells of the endometrial lesions, partially or totally co-localizing with iron deposits. These observations suggest some endocrine disrupting chemical

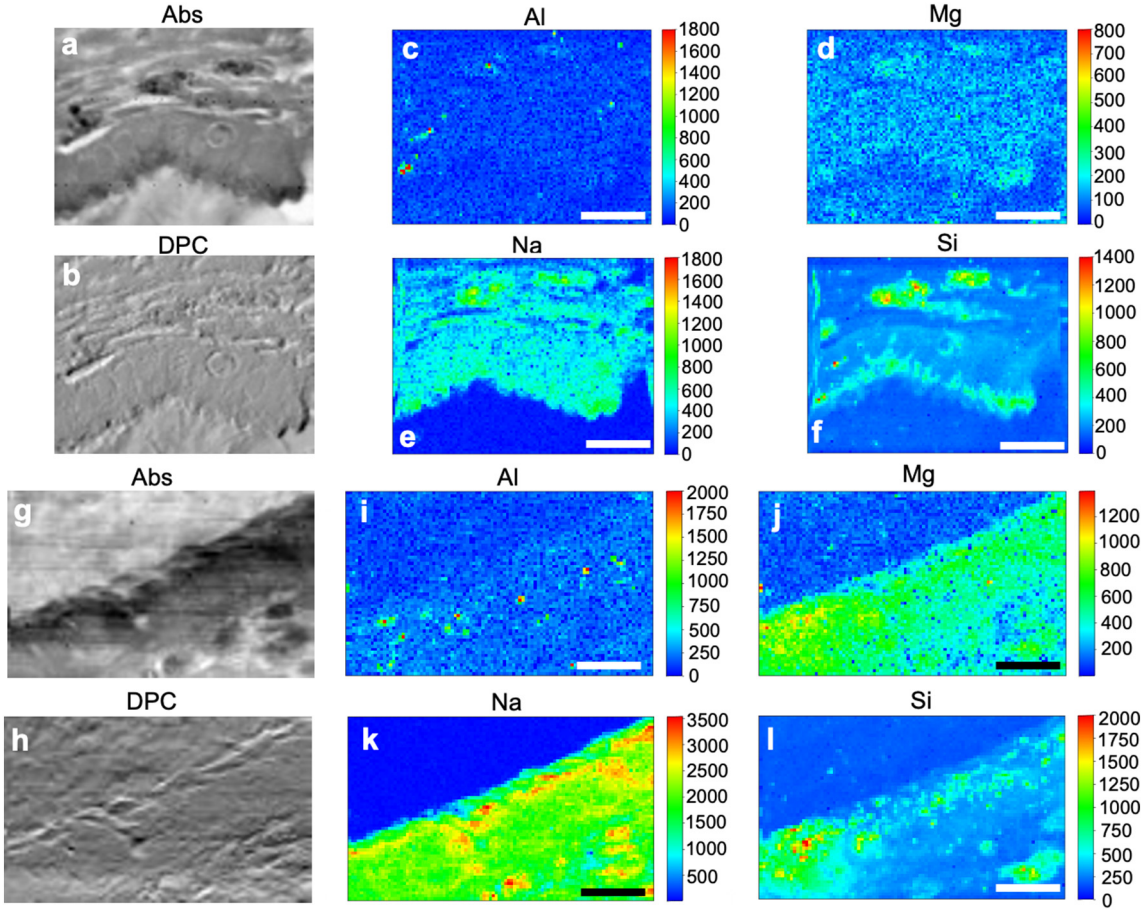

Fig. 10. X-ray microscopy absorption (a,g) and phase contrast (b,h) images and the corresponding Al (c, i panels), Mg (d, j panels), Na (e, k panels), Si (f, l panels) XRF intensity maps of an endometrial tissue of patient A18 (scale bar 20 μm). All images were collected at 2 keV with a step size of 400 nm and 5 s/pixel acquisition time.

elements are related to iron dysmetabolism and may be involved in triggering or favoring the progression of the disease Further studies are needed to expand these novel observations, focusing on the mechanism of metals accumulation in tissues in relation to iron dysmetabolism (Ng et al., 2020), as to defend and advance the theory of endocrine disrupting chemicals involved in endometriosis.

Funding statement

This work was supported by Ministry of Health, Italy (RC ENDO-2020-23670288) and by IRCCS-Burlo Garofolo (5mille15D7).

Attestation statement

- Data regarding any of the subjects in the study has not been previously published unless specified.
- Data will be made available to the editors of the journal for review or query upon request.

CRediT authorship contribution statement

Lorella Pascolo: Conceptualization, Methodology, Writing-Original draft preparation, Investigation, Funding. **Maria Pachetti**: Writing-Original draft preparation, Investigation, Data curation. **Anna Camillo**: Investigation, Data curation. **Alice Cernogoraz**: Investigation. **Clara Rizzardi**: Investigation, Writing - Review & Editing. **Katarina Vogel Mikus**: Formal analyses, Writing - Review & Editing. **Fabrizio Zanconati**: Validation, Supervision. **Murielle Salomé**: Software, Validation, Writing - Review & Editing. **Vanessa Tardillo Suárez:** Software, Validation. **Federico Romano**: Validation, **Gabriella Zito**: Validation, Writing - Review & Editing. **Alessandra Gianoncelli**: Methodology, Investigation, Writing - Review & Editing. **Giuseppe Ricci:** Conceptualization, Supervision, Writing - Review & Editing, Funding.

Data availability

Data will be made available on request.

Declaration of competing interest

The authors declare that they have no known competing financial interests or personal relationships that could have appeared to influence the work reported in this paper.

Acknowledgment

We acknowledge the European Synchrotron Radiation Facility for provision of synchrotron radiation facilities during experiment MD-1113 at beamline ID21. We acknowledge Elettra Sincrotrone Trieste (Trieste, Italy) for granting access to its synchrotron radiation facility and the TwinMic beamline. The authors thank Martina Bradaschia for the English revision of the manuscript.

Appendix A. Supplementary data

Supplementary data to this article can be found online at https://doi.org/10.1016/j.scitotenv.2022.161028.

References

Bissardon, C., Reymond, S., Salomé, M., André, L., Bayat, S., Cloetens, P., Bohic, S., 2019. Cell culture on silicon nitride membranes and cryopreparation for synchrotron X-ray fluorescence nano-analysis. J. Vis. Exp. https://doi.org/10.3791/60461.

Brosens, I., Puttemans, P., Campo, R., Gordts, S., Kinkel, K., 2004. Diagnosis of endometriosis: pelvic endoscopy and imaging techniques. Best Pract. Res. Clin. Obstet. Gynaecol. 18, 285–303. https://doi.org/10.1016/j.bpobgyn.2004.03.002.

Bulun, S.E., 2009. Endometriosis. N. Engl. J. Med. 360, 268–279. https://doi.org/10.1056/NEJMra0804690.

Choe, S.-Y., Kim, S.-J., Kim, H.-G., Lee, J.H., Choi, Y., Lee, H., Kim, Y., 2003. Evaluation of estrogenicity of major heavy metals. Sci. Total Environ. 312, 15–21. https://doi.org/10.1016/S0048-9697(03)00190-6.

Cousins, F.L., O, D.F., Gargett, C.E., 2018. Endometrial stem/progenitor cells and their role in the pathogenesis of endometriosis. Best Pract. Res. Clin. Obstet. Gynaecol. 50, 27–38. https://doi.org/10.1016/j.bpobgyn.2018.01.011.

Darbre, P.D., 2006. Metalloestrogens: an emerging class of inorganic xenoestrogens with potential to add to the oestrogenic burden of the human breast. J. Appl. Toxicol. 26, 191–197. https://doi.org/10.1002/jat.1135.

Defrère, S., Lousse, J.C., González-Ramos, R., Colette, S., Donnez, J., Van Langendonckt, A., 2008. Potential involvement of iron in the pathogenesis of peritoneal endometriosis. Mol. Hum. Reprod. 14, 377–385. https://doi.org/10.1093/molehr/gan033.

Delfino, R., Altissimo, M., Menk, R.H., Alberti, R., Klatka, T., Frizzi, T., Longoni, A., Salomè, M., Tromba, G., Arfelli, F., Clai, M., Vaccari, L., Lorusso, V., Tiribelli, C., Pascolo, L., 2011. X-ray fluorescence elemental mapping and microscopy to follow hepatic disposition of a Gd-based magnetic resonance imaging contrast agent. Clin. Exp. Pharmacol. Physiol. 38, 834–845. https://doi.org/10.1111/j.1440-1681.2011.05618.x.

Delfino, R., Biasotto, M., Candido, R., Altissimo, M., Stebel, M., Salomè, M., van Elteren, J.T., Vogel Mikuš, K., Zennaro, C., Šala, M., Addobbati, R., Tromba, G., Pascolo, L., 2019. Gadolinium tissue deposition in the periodontal ligament of mice with reduced renal function exposed to Gd-based contrast agents. Toxicol. Lett. 301, 157–167. https://doi.org/10.1016/j.toxlet.2018.11.014.

Ghio, A.J., Soukup, J.M., Dailey, L.A., Richards, J.H., Turi, J.L., Pavlisko, E.N., Roggli, V.L., 2012. Disruption of iron homeostasis in mesothelial cells after talc pleurodesis. Am. J. Respir. Cell Mol. Biol. 46, 80–86. https://doi.org/10.1165/rcmb.2011-0168OC.

Gianoncelli, A., Kaulich, B., Alberti, R., Klatka, T., Longoni, A., De Marco, A., Marcello, A., Kiskinova, M., 2009. Simultaneous soft X-ray transmission and emission microscopy. Nucl. Instrum. Methods Phys. Res., Sect. A 608, 195–198. https://doi.org/10.1016/j.nima.2009.06.035.

Gianoncelli, A., Kourousias, G., Merolle, L., Altissimo, M., Bianco, A., 2016. Current status of the TwinMic beamline at Elettra: a soft X-ray transmission and emission microscopy station. J. Synchrotron Radiat. 23, 1526–1537. https://doi.org/10.1107/S1600577516014405.

Gianoncelli, A., Kourousias, G., Stolfa, A., Kaulich, B., 2013. Recent developments at the TwinMic beamline at ELETTRA: an 8 SDD detector setup for low energy X-ray fluorescence. J. Phys. Conf. Ser. 425, 182001. https://doi.org/10.1088/1742-6596/425/18/182001.

Gianoncelli, A., Morrison, G.R., Kaulich, B., Bacescu, D., Kovac, J., 2006. Scanning transmission X-ray microscopy with a configurable detector. Appl. Phys. Lett. 89, 251117. https://doi.org/10.1063/1.2422908.

González-Ramos, R., Defrère, S., Devoto, L., 2012. Nuclear factor–kappaB: a main regulator of inflammation and cell survival in endometriosis pathophysiology. Fertil. Steril. 98, 520–528. https://doi.org/10.1016/j.fertnstert.2012.06.021.

Hagenfeldt, K., Landgren, B.M., Plantin, L.O., Diczfalusy, E., 1977. Trace elements in the human endometrium and decidua.A multielement analysis. Acta Endocrinol. 85, 406–414. https://doi.org/10.1530/acta.0.0850406 (Copenh).

Ito, F., Kato, K., Yanatori, I., Murohara, T., Toyokuni, S., 2021. Ferroptosis-dependent extracellular vesicles from macrophage contribute to asbestos-induced mesothelial carcinogenesis through loading ferritin. Redox Biol. 47, 102174. https://doi.org/10.1016/j.redox.2021.102174.

Kaulich, B., Gianoncelli, A., Beran, A., Eichert, D., Kreft, I., Pongrac, P., Regvar, M., Vogel-Mikuš, K., Kiskinova, M., 2009. Low-energy X-ray fluorescence microscopy opening new opportunities for bio-related research. J. R. Soc. Interface 6, S641–S647. https://doi.org/10.1098/rsif.2009.0157.focus.

Koren, Š., Arčon, I., Kump, P., Nečemer, M., Vogel-Mikuš, K., 2013. Influence of CdCl2 and CdSO4 supplementation on Cd distribution and ligand environment in leaves of the Cd hyperaccumulator Noccaea (Thlaspi) praecox. Plant Soil 370, 125–148. https://doi.org/10.1007/s11104-013-1617-0.

Kump, P., Vogel-Mikuš, K., 2018. Quantification of 2D elemental distribution maps of intermediate-thick biological sections by low energy synchrotron $\upmu$-X-ray fluorescence spectrometry. J. Inst. 13. https://doi.org/10.1088/1748-0221/13/05/C05014 C05014-C05014.

Maximova, N., Gregori, M., Zennaro, F., Sonzogni, A., Simeone, R., Zanon, D., 2016. Hepatic gadolinium deposition and reversibility after contrast agent-enhanced MR imaging of pediatric hematopoietic stem cell transplant recipients. Radiology 281, 418–426. https://doi.org/10.1148/radiol.2016152846.

Milic, S., Mikolasevic, I., Orlic, L., Devcic, E., Starcevic-Cizmarevic, N., Stimac, D., Kapovic, M., Ristic, S., 2016. The role of iron and iron overload in chronic liver disease. Med. Sci. Monit. 22, 2144–2151. https://doi.org/10.12659/MSM.896494.

Morassutto, C., Monasta, L., Ricci, G., Barbone, F., Ronfani, L., 2016. Incidence and estimated prevalence of endometriosis and adenomyosis in Northeast Italy: a data linkage study. PLoS One 11, e0154227. https://doi.org/10.1371/journal.pone.0154227.

Mori, M., Ito, F., Shi, L., Wang, Y., Ishida, C., Hattori, Y., Niwa, M., Hirayama, T., Nagasawa, H., Iwase, A., Kikkawa, F., Toyokuni, S., 2015. Ovarian endometriosis-associated stromal cells reveal persistently high affinity for iron. Redox Biol. 6, 578–586. https://doi.org/10.1016/j.redox.2015.10.001.

Nakamura, T., Naguro, I., Ichijo, H., 2019. Iron homeostasis and iron-regulated ROS in cell death, senescence and human diseases. Biochim. Biophys. Acta Gen. Subj. 1863, 1398–1409. https://doi.org/10.1016/j.bbagen.2019.06.010.

Ng, S.-W., Norwitz, S.G., Taylor, H.S., Norwitz, E.R., 2020. Endometriosis: the role of iron overload and ferroptosis. Reprod. Sci. 27, 1383–1390. https://doi.org/10.1007/s43032-020-00164-z.

Ortega, R., Cloetens, P., Devès, G., Carmona, A., Bohic, S., 2007. Iron storage within dopamine neurovesicles revealed by chemical nano-imaging. PLoS ONE 2, e925. https://doi.org/10.1371/journal.pone.0000925.

Osuchowska-Grochowska, I., Blicharska, E., Gogacz, M., Nogalska, A., Winkler, I., Szopa, A., Ekiert, H., Tymczyna-Borowicz, B., Rahnama-Hezavah, M., Grochowski, C., 2021. Brief review of endometriosis and the role of trace elements. Int. J. Mol. Sci. 22, 11098. https://doi.org/10.3390/ijms222011098.

Pascolo, L., Borelli, V., Canzonieri, V., Gianoncelli, A., Birarda, G., Bedolla, D.E., Salomé, M., Vaccari, L., Calligaro, C., Cotte, M., Hesse, B., Luisi, F., Zabucchi, G., Melato, M., Rizzardi, C., 2015. Differential protein folding and chemical changes in lung tissues exposed to asbestos or particulates. Sci. Rep. 5, 12129. https://doi.org/10.1038/srep12129.

Pascolo, L., Gianoncelli, A., Rizzardi, C., Tisato, V., Salomé, M., Calligaro, C., Salvi, F., Paterson, D., Zamboni, P., 2014. Calcium micro-depositions in jugular truncular venous malformations revealed by Synchrotron-based XRF imaging. Sci. Rep. 4, 6540. https://doi.org/10.1038/srep06540.

Pascolo, L., Gianoncelli, A., Schneider, G., Salomé, M., Schneider, M., Calligaro, C., Kiskinova, M., Melato, M., Rizzardi, C., 2013. The interaction of asbestos and iron in lung tissue revealed by synchrotron-based scanning X-ray microscopy. Sci. Rep. 3. https://doi.org/10.1038/srep01123.

Patel, B.G., Rudnicki, M., Yu, J., Shu, Y., Taylor, R.N., 2017. Progesterone resistance in endometriosis: origins, consequences and interventions. Acta Obstet. Gynecol. Scand. 96, 623–632. https://doi.org/10.1111/aogs.13156.

Paunesku, T., Vogt, S., Maser, J., Lai, B., Woloschak, G., 2006. X-ray fluorescence microprobe imaging in biology and medicine. J. Cell. Biochem. 99, 1489–1502. https://doi.org/10.1002/jcb.21047.

Paunesku, T., Wanzer, M.B., Kirillova, E.N., Muksinova, K.N., Revina, V.S., Romanov, S.A., Lyubchansky, E.R., Grosche, B., Birschwilks, M., Vogt, S., Finney, L., Woloschak, G.E., 2012. X-ray fluorescence microscopy for investigation of archival tissues. Health Phys. 103, 181–186. https://doi.org/10.1097/HP.0b013e31824e7023.

Pollack, A.Z., Louis, G.M.B., Chen, Z., Peterson, C.M., Sundaram, R., Croughan, M.S., Sun, L., Hediger, M.L., Stanford, J.B., Varner, M.W., Palmer, C.D., Steuerwald, A.J., Parsons, P.J., 2013. Trace elements and endometriosis: the ENDO study. Reprod. Toxicol. 42, 41–48. https://doi.org/10.1016/j.reprotox.2013.05.009.

Ralle, M., Lutsenko, S., 2009. Quantitative imaging of metals in tissues. Biometals 22, 197–205. https://doi.org/10.1007/s10534-008-9200-5.

Rockfield, S., Raffel, J., Mehta, R., Rehman, N., Nanjundan, M., 2017. Iron overload and altered iron metabolism in ovarian cancer. Biol. Chem. 398, 995–1007. https://doi.org/10.1515/hsz-2016-0336.

Rzymski, Piotr, Niedzielski, P., Rzymski, Paweł, Tomczyk, K., Kozak, L., Poniedziałek, B., 2016. Metal accumulation in the human uterus varies by pathology and smoking status. Fertil. Steril. 105, 1511–1518.e3. https://doi.org/10.1016/j.fertnstert.2016.02.006.

Rzymski, Piotr, Tomczyk, K., Rzymski, Pawel, Poniedziałek, B., Opala, T., Wilczak, M., 2015. Impact of heavy metals on the female reproductive system. Ann. Agric. Environ. Med. 22, 259–264. https://doi.org/10.5604/12321966.1152077.

Scutiero, G., Iannone, P., Bernardi, G., Bonaccorsi, G., Spadaro, S., Volta, C.A., Greco, P., Nappi, L., 2017. Oxidative stress and endometriosis: a systematic review of the literature. Oxidative Med. Cell. Longev. 2017, 7265238. https://doi.org/10.1155/2017/7265238.

Silva, N., Senanayake, H., Peiris-John, R., Wickremasinghe, R., Sathiakumar, N., Waduge, V., 2012. Presence of metalloestrogens in ectopic endometrial tissue. J. Pharm. Biomed. Sci. 24, 1–5.

Sirohi, D., Ramadhani, R.A., Knibbs, L.D., 2021. Environmental exposures to endocrine disrupting chemicals (EDCs) and their role in endometriosis: a systematic literature review. Rev. Environ. Health 36, 101–115. https://doi.org/10.1515/reveh-2020-0046.

Smarr, M.M., Kannan, K., Buck Louis, G.M., 2016. Endocrine disrupting chemicals and endometriosis. Fertil. Steril. 106, 959–966. https://doi.org/10.1016/j.fertnstert.2016.06.034.

Sole, A., Papillon, E., Cotte, M., Walter, P., Susini, J., 2007. A multiplatform code for the analysis of energy-dispersive X-ray fluorescence spectra. Spectrochim. Acta B At. Spectrosc. 62, 63–68. https://doi.org/10.1016/j.sab.2006.12.002.

Tanrıkut, E., Karaer, A., Celik, O., Celik, E., Otlu, B., Yilmaz, E., Ozgul, O., 2014. Role of endometrial concentrations of heavy metals (cadmium, lead, mercury and arsenic) in the aetiology of unexplained infertility. Eur.J.Obstet.Gynecol.Reprod.Biol. 179, 187–190. https://doi.org/10.1016/j.ejogrb.2014.05.039.

Wang, X., Xia, T., 2015. New insights into disruption of iron homeostasis by environmental pollutants. J. Environ. Sci. 34, 256–258. https://doi.org/10.1016/j.jes.2015.06.001.

Wang, Y., Nicholes, K., Shih, I.-M., 2020. The origin and pathogenesis of endometriosis. Annu. Rev. Pathol. 15, 71–95. https://doi.org/10.1146/annurev-pathmechdis-012419-032654.

Wiegerinck, M.A., Van Dop, P.A., Brosens, I.A., 1993. The staging of peritoneal endometriosis by the type of active lesion in addition to the revised American Fertility Society classification. Fertil. Steril. 60, 461–464. https://doi.org/10.1016/s0015-0282(16)56161-5.

Wölfler, M.M., Meinhold-Heerlein, I.M., Henkel, C., Rath, W., Neulen, J., Maass, N., Bräutigam, K., 2013. Reduced hemopexin levels in peritoneal fluid of patients with endometriosis. Fertil. Steril. 100, 777–781. https://doi.org/10.1016/j.fertnstert.2013.05.010.

Ying, J.-F., Lu, Z.-B., Fu, L.-Q., Tong, Y., Wang, Z., Li, W.-F., Mou, X.-Z., 2021. The role of iron homeostasis and iron-mediated ROS in cancer. Am. J. Cancer Res. 11, 1895–1912.

Zondervan, K.T., Becker, C.M., Missmer, S.A., 2020. Endometriosis. N. Engl. J. Med. https://doi.org/10.1056/NEJMra1810764.